Chapter 27
Mode Shape Comparison Using Continuous-Scan Laser Doppler Vibrometry and High Speed 3D Digital Image Correlation

David A. Ehrhardt, Shifei Yang, Timothy J. Beberniss, and Matthew S. Allen

Abstract Experimental structural dynamic measurements are traditionally obtained using discrete sensors such as accelerometers, strain gauges, displacement transducers, etc. These techniques are known for providing measurements at discrete points. Also, a majority of these sensors require contact with the structure under test which may modify the dynamic response. In contrast, a few recently developed techniques are capable of measuring the response over a wide measurement field without contacting the structure. Two techniques are considered here: continuous-scan laser Doppler vibrometry (CSLDV) and high speed three dimensional digital image correlation (3D-DIC). The large amount of measured velocities and displacements provide an unprecedented measurement resolution; however, they both require post processing to obtain measurements. In this investigation, the frequency response function of a clamped-clamped flat beam will be determined using a modal hammer test, CSLDV, and high speed 3D-DIC. The mode shapes of the beam determined by each of these experimental methods will then be compared to assess the relative merits of each measurement approach.

Keywords Continuous scan laser • Digital image correlation

27.1 Introduction

The development of full-field measurement techniques has received much attention as the design of high-performance light weight structures has advanced. There is an increasing need for experimental techniques capable of measuring the response at a large number of measurement degrees of freedom without modifying the structural response significantly, and techniques such as Continuous-Scan Laser Doppler Vibrometry (CSLDV) and high-speed Three Dimensional Digital Image Correlation (high-speed 3D-DIC) have been developed to meet this need. Both CSLDV and high-speed 3D-DIC are capable of measuring the response at thousands of points across the surface of the test specimen with good accuracy. However, these techniques involve additional processing to extract velocities or displacements when compared with traditional measurement techniques.

Measurements from CSLDV are more challenging to process than traditional Laser Doppler Vibrometer (LDV) measurements because in CSLDV, the measurement point is continuously moving during the measurement, so the system must be treated as time-varying. The benefit provided by the continuously moving measurement point is an increased measurement resolution with a drastically decreased measurement time when compared with a traditional LDV measurements, which must remain at a measurement location for a prescribed length of time. Various algorithms have been devised to determine the mode shapes of the test piece along a continuously moving laser scan path. For example, Ewins et al. treated the operational deflection shape as a polynomial function of the moving laser position [1–5]. They showed that sideband harmonics appear in the measured spectrum, each separated by the scan frequency, and that the amplitudes of the sidebands can be used to determine the polynomial coefficients. Allen et al. later presented a lifting approach for impulse response measurements [6, 7]. The lifting approach groups the responses at the same location along the laser path. Hence, the lifted responses appear to be from a set of pseudo sensors attached to the structure, allowing conventional modal analysis routines to extract

D.A. Ehrhardt (✉) • S. Yang • M.S. Allen
Department of Engineering Physics, University of Wisconsin-Madison, 535 Engineering Research Building, 1500 Engineering Drive, Madison, WI 53706, USA
e-mail: dehrhardt@wisc.edu

T.J. Beberniss
Structural Sciences Centers, Aerospace Systems Directorate, Air Force Research Laboratory, Wright-Patterson AFB, Dayton, OH 45433, USA

G. Foss and C. Niezrecki (eds.), *Special Topics in Structural Dynamics, Volume 6: Proceedings of the 32nd IMAC, A Conference and Exposition on Structural Dynamics, 2014*, Conference Proceedings of the Society for Experimental Mechanics Series,
DOI 10.1007/978-3-319-04729-4_27,

modal parameters from the CSLDV measurements. Recently, algorithms based on Linear Time Periodic (LTP) system theory [8–11] were used to derive input–output transfer functions from CSLDV measurements allowing virtually any input to be used with CSLDV. These algorithms will be used in this investigation to identify the natural frequencies and modes shapes of a clamped-clamped beam.

Displacements measured with 3D-DIC are challenging to obtain since each individual measurement point has to be matched in each image from each camera for the duration of the experiment. For sample rates greater than 100 fps, this requires an additional step of post processing. Schmidt et al. [12] presented early work on the use of high-speed digital cameras to measure deformation and strain experienced by test articles under impact loadings. Tiwari et al. [13] used two high-speed CMOS cameras in a stereo-vision setup to measure the out of plane displacement of a plate subjected to a pulse input. Results compared favorably with work previously published and showed the capability of the 3D-DIC system in a high-speed application, although over a short time history. Niezrecki et al. [14], Helfrick et al. [15], and Warren et al. [16] obtained mode shapes using 3D-DIC with different test articles using discrete measuring points. Niezrecki et al. and Helfrick et al. also combined accelerometers, vibrometers, and dynamic photogrammetry to compare results obtained with DIC analyzed at discrete measurement locations. Each technique provided complimentary between all measurement techniques showing the capability of 3D-DIC, although 3D-DIC was not processed along the entire surface. Since 3D-DIC has the capability to measure hundreds of 3D displacements on a surface, a further comparison can be made with full field measurements; however handling the large amount of data in conjunction with the image files can prove to be difficult.

In this investigation, CSLDV and high-speed 3D-DIC are used to measure the linear dynamic response of a 9″ mild steel clamped-camped beam. For comparison, the response of the specified beam is measured when it is excited with a steady state sinusoid at the first three measured natural frequencies and when it is excited with a band limited random excitation from 10 to 800 Hz. To process measurements from CSLDV, both the harmonic transfer function and harmonic power spectrum will be used to identify mode shapes of the clamped-clamped beam under the sinusoidal and random excitation, respectively. Displacements measured by 3D-DIC are processed using a commercial software Aramis [17] and its Real Time Sensor program [18]. In both CSLDV and 3D-DIC, mode shapes and natural frequencies are extracted from the assembled transfer function using peak picking for the steady state excitation and the Algorithm of Mode Isolation (AMI) [19] for the random excitation.

27.2 Measurements

27.2.1 CSLDV Theory/Mode Shape Extraction Description

The CSLDV measurements were acquired using a periodic scan pattern, e.g., a line as shown in Fig. 27.1, so the measurements appear to be from a linear time periodic (LTP) system because the measurement location is moving periodically [19].

In this work, the harmonic transfer function and harmonic power spectrum concepts from LTP systems theory will be employed to process CSLDV measurements in order to extract the modal parameters of the beam. These algorithms are completely analogous to the transfer function and power spectrum of linear time invariant (LTI) systems; both the harmonic transfer function and harmonic power spectrum can be written in a modal summation form in terms of the modal parameters of the clamped beam. Therefore the well-established LTI modal identification routines can be used to process CSLDV measurements.

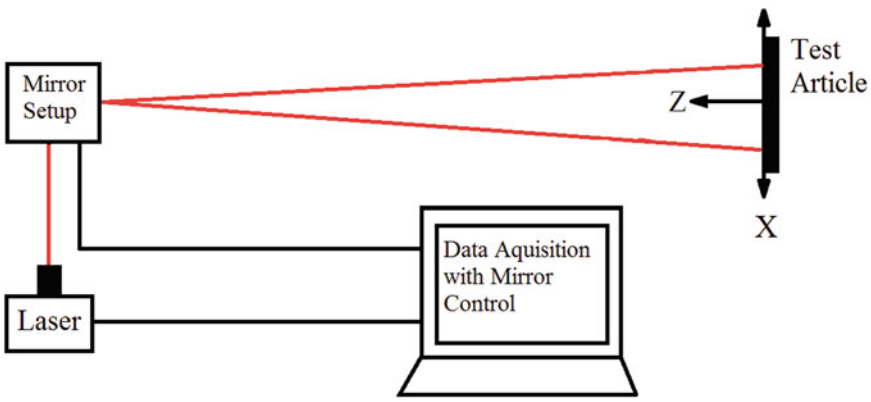

Fig. 27.1 CSLDV system diagram: the laser beam was redirect by a pair of mirror to continuously scan on the test article

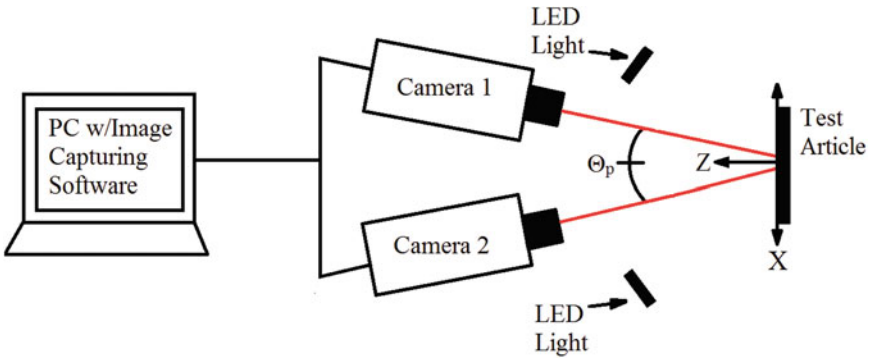

Fig. 27.2 3D-DIC system diagram. The 3D-DIC system diagram shows Camera 1 (left camera) and Camera 2 (right camera) set to a specified pan angle, Θ_p

However, there are two notable differences. First, the mode vectors ψ_r of an LTI system describe the spatial pattern of deformation of a mode over the set of measurement points. In contrast, when using CSLDV to measure mode shapes of a structure, one has a moving measurement point. The location of that point is expanded in the processing step so that the mode vectors $\overline{\mathbf{C}}_{r,l}$ end up consisting of a vector of the Fourier coefficients $\overline{C}_{r,n}$ that describe the time periodic spatial deformation pattern along the scan path, $C(t)\psi_r = \sum_{n=-\infty}^{\infty} \overline{C}_{r,n} e^{jn\omega_A t}$, where $C(t)$ is an output vector indicating the location where the response is being measured at any instant, and ω_A is the laser scanning frequency. Second, an LTP system theoretically has an infinite number of peaks for each mode. Each peak occurs near the imaginary part of the Floquet exponent λ_r plus some integer multiple of the fundamental frequency ω_A. If the observed mode shapes $C(t)\psi_r$ are constant in time (the laser is stationary), $\overline{\mathbf{C}}_{r,l}$ would contain only one nonzero term, and the system reduces to the familiar linear time invariant system. Note that one needs to fit a peak to each harmonic of each mode to obtain a best estimate of the mode vector [20].

The harmonic transfer function and harmonic power spectrum are readily derived by defining an exponentially modulated periodic signal and then using the general solution for the response of a linear time varying system. The readers are referred to [19] for more details about the derivation.

27.2.2 DIC Theory/Mode Shape Extraction Description

To accurately measure 3D displacements with DIC, a setup using two cameras is used to image the test article as it deforms. As shown in Fig. 27.2, the two cameras are placed at a specific distance along the Z-axis from the test article to allow the surface to be captured simultaneously in each camera and establish a field of view. A pan angle, Θ_p, is specified based on a desired depth of view or range of out-of-plane displacements expected. Once the stereo camera setup is assembled and fixed, photogrammetric principles of triangulation and bundle adjustment are used to establish each camera's position and the experimental measurement volume by capturing images of a known pattern or calibration panel [21]. With this calibration, displacement accuracy is not limited to the pixel size of the imaged surface of the test specimen, but instead allows for accuracies on the sub pixel level (e.g. 0.01 pixels). Additionally, in-plane deformations are measured with a greater accuracy when compared with purely out-of-plane deformations. Prior to testing, a high-contrast random gray-scale pattern is applied to the measurement surface so facets from each image can be matched. As detailed in [21], triangulation of the facet and surface matching is used to determine the coordinate value of each measurement point.

27.3 Experimental Setup

27.3.1 Beam Description

The device under test for this investigation is a precision-machined flat feeler gauge made from high-carbon, spring-steel in a clamped-clamped configuration. As summarized in Table 27.1, the tested beam had an effective length of 9 in., a nominal width of 0.5 in., and a thickness of 0.03 in. Prior to clamping, the beam was painted with a white base coat and a speckle pattern was applied using a marker to allow for tracking positions with the 3D-DIC system. Once the beam had dried, a strip

Table 27.1 Beam geometric and material properties

Length = 9 in.	Width = 0.5 in.	Thickness = 0.031 in.
E = 29.7 Mpsi	G = 11.6 Mpsi	Rho = 7.36×10^{-4} lb-s^2/in^4

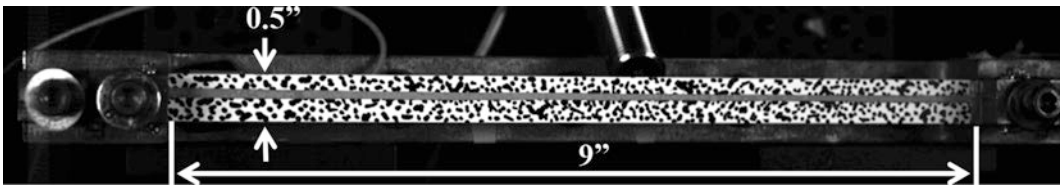

Fig. 27.3 Beam specimen

of retro-reflective tape was added to increase feedback for the CSLDV. The final prepared beam is shown in the clamping fixture in Fig. 27.3. The clamping force was provided by the two 6.35-28 UNF-2B bolts located on the inside of the clamping fixture, which is the same fixture used in [22]. Both inside bolts were tightened to 90 in.-lbs; however, the outer bolts were not tightened to the full 90 in.-lbs due to the noticeable deformation of the beam during clamping. Static 3D-DIC images were captured during clamping to quantify any initial deflection seen. It is noted that the 3D-DIC deformation measurements during clamping are approaching the noise floor of the system for this field of view; however, maximum deformations measured during clamping are below 25 % of the beam thickness. Since 3D-DIC is sensitive to small deformations, the beam was driven at the largest force that allowed a linear response. This force was determined by incrementally increasing the input force level while monitoring damping. When damping increased a measurable amount, the force was decreased to the previous forcing level. The maximum resulting response was 62 % of the beam thickness.

27.3.2 Experimental Setup

Figure 27.4 shows the experimental setup. The continuous-scan mechanisms were built using a Polytec OFV-552 fiber optic laser vibrometer with a sensitivity of 125 mm/s/V and the same external mirror system that was used in [19, 23, 24]. It is worth noting that a fiber optic laser such as this has not been used with CSLDV in any of the authors' previous works. The external mirror system consisted of two galvanometer scanners in closed-loop control; each scanner had a position detector that measured the instantaneous rotational angle, allowing precise and accurate control of the laser position. The control and data acquisition system was built using a National Instruments PXI system. A LabVIEW program was developed to integrate several the features including the function generator, data acquisition, and signal processing.

The 3D-DIC system includes two Photron, high speed 12-bit CMOS cameras (model Fastcam SA5 775K-M3K). Each camera has onboard 32GBs of memory with a maximum resolution of $1{,}024 \times 1{,}024$ pixels. For this experimental setup, images of 832×144 pixels were used. All static displacements were calculated using a commercial 3D-DIC software Aramis [17], while dynamic displacements were calculated using a software extension of Aramis called IVIEW Real Time Sensor [18]. In order to minimize the heat generated and remove the 60 Hz noise produced by halogen lamps typically used in high-speed DIC systems, two panel, 100×100 LED lights were used. The cameras and the data acquisition system were simultaneously started using an external TTL trigger.

As previously stated, Aramis in combination with the Real Time Sensor module is used to post-process the images and extract the measured displacements. Due to limited processing time with the 3D-DIC software, only two rows of 41 points along the beam were selected to be processed for this investigation. One row of measurement points is located above the laser scan retro reflective tape shown in Fig. 27.3 and the other is below the tape. A maximum of 2,500 points in a 2D grid across the surface of the beam could have been processed if time permitted. Also, since all images were stored, the data can be reprocessed to obtain a denser measurement grid if needed. A 250 mm $\times$ 200 mm calibration panel was used to establish the measurement volume and lead to a calibration deviation of 0.02 pixels or 0.007 mm based on the field of view. To process the displacements, a facet size of 20 pixel $\times$ 20 pixel was used. After processing the recorded images and obtaining the displacements, the frequency response function (FRF) was calculated from the auto and cross spectrum determined using the Fourier transform in MATLAB. Using peak picking, the imaginary part of the FRFs for the steady state response was used to determine the mode shapes. AMI was used to extract the mode shapes and natural frequencies from the random response data after 45 averages with a block size of 5,000 samples and a 50 % overlap.

The steady state sinusoidal input was provided by a magnetic driver with a Piezo Amplifier in line with a Wavetek Variable Phase Synthesizer. To measure the force provided by the magnetic driver, a force transducer measured the reaction

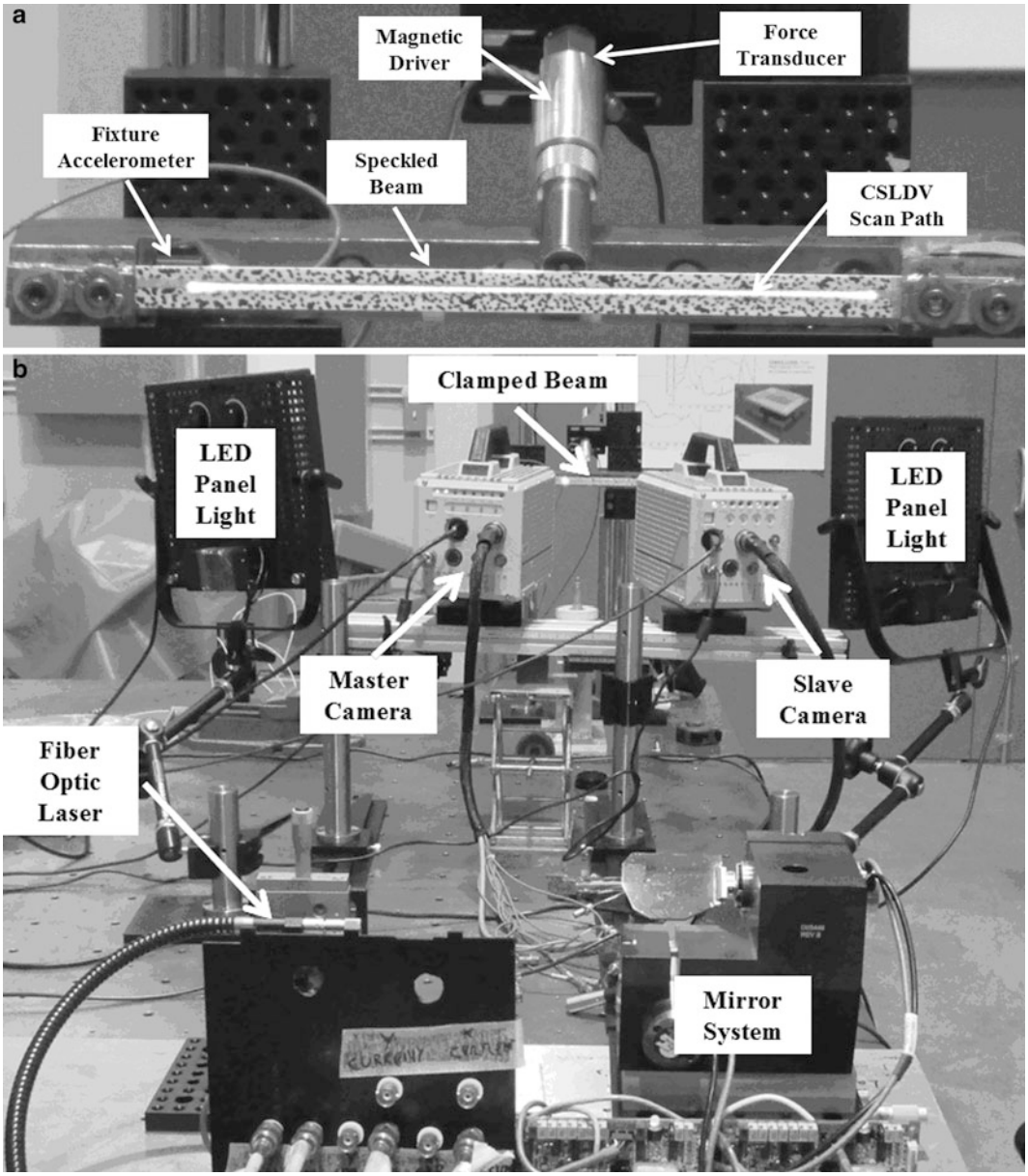

Fig. 27.4 Experimental setup. (**a**) Close up of clamped beam, (**b**) Complete experimental setup

force between the magnetic driver and the frame to which it was mounted. In addition to the steady state experiments at the natural frequencies of the beam, a band limited random excitation was used over the range of 10–800 Hz. The same magnetic driver was used to provide the band limited random excitation.

Prior to sinusoidal and random excitation testing, a modal survey was performed using a modal hammer and a single point laser to establish the natural frequencies and damping ratios of the clamped-clamped beam. The first three identified natural frequencies were used as driving frequencies for the steady state sinusoidal tests. For steady state experiments, the CSLDV system scanned the surface of the beam at 3 Hz with a sampling frequency of 5,120 Hz. The total scan time was 2 min. The high-speed 3D-DIC system captured 40,000 images at 2,000 fps. The total measurement time was 20 s, but an additional 10 min was needed to download the images from the cameras. For the random excitation experiment, the CSLDV system scanned the surface of the beam at 9 Hz with a sampling frequency of 5,120 for a duration of 15 min. The high-speed 3D-DIC system captured 120,000 images at 5,000 fps, and an additional 40 min was needed to download all images from the cameras. The input signals were not recorded in these tests, so the longer time histories used for these tests allowed for more averaging to reduce the noise and variability in the response due to the random input force.

27.4 Results

27.4.1 Modal Hammer Test

A single input and single output modal hammer test was performed on the beam to identify the first three natural frequencies and document any frequency shifts during testing. Pre- and postexcitation modal hammer tests for the steady state sine experiments showed a small frequency shift of 0.5 Hz for the first three modes of the beam. Similarly a frequency shift of 2 Hz, 2.5 Hz, and 3.5 Hz was observed for modes 1, 2, and 3 for the pre- and postexcitation modal hammer tests for the random experiments. Since the temperature difference between the beam and the fixture remained less than 1 °C for all tests, the larger observed frequency shifts in the random excitation experiment were concluded to be a result of a change in boundary conditions, perhaps due to the clamped ends of the beam slightly slipping as it was excited. The clamed beam has been shown to be very sensitive to slight temperature changes [22], which could account for some of the observed shift in natural frequencies. The average of each natural frequency identified with the modal hammer tests was compared with the natural frequencies identified using CSLDV and high-speed 3D-DIC and the results are shown in Table 27.2. The computed MAC values for the mode shapes determined from testing are also shown in Table 27.2, but will be discussed later. The maximum difference between the natural frequencies measured by each method was 2.6 % although most differed by less than 1 %. It is worth noting that the percent difference between the natural frequencies measured with CSLDV and 3D-DIC were within the observed percent change between the pre- and postmodal tests, leading to the conclusion that test setup variability is a major part in the differences between the identified natural frequencies.

27.4.2 Mode Shape Comparison: Sine Dwell Experiments

As previously mentioned, the beam was driven at each of the first three identified natural frequencies and the steady state response was measured using both CSLDV and high-speed 3D-DIC. Figure 27.5a shows an example of the spectrum from the CSLDV signal with the laser scanning at 3 Hz when the beam was driven at 71.3 Hz. The sideband harmonics higher than the 6th order are buried in the noise floor and hence no harmonics above the 6th order were used when construction the mode shape. The harmonic transfer function was computed using $n = -8{:}8$ to assure that all of these harmonics were captured. Figure 27.5b shows the magnitude and phase of the Fourier coefficients obtained by peak picking at 71.3 Hz versus the harmonic order. Note that there is a small phase error (about 0.5°) between any neighboring peaks which could be caused by the mirror phase delay [25]. These Fourier coefficients for harmonics of $n = -6{:}6$ were then used to construct the mode shape along the laser path. The second and third bending mode shapes were reconstructed using the Fourier coefficients for harmonics $n = -10$ to 10 and $n = -15$ to 15, respectively.

Figure 27.6 compares the mode shapes obtained by CSLDV and DIC for the three steady state experiments. Figure 27.6a contains the mode shape at 71.3 Hz and shows the difference between the mode shapes measured with CSLDV and the upper and lower row of measurement points obtained with high-speed 3D-DIC. Similarly, Fig. 27.6b, c shows the mode shapes at 205.5 Hz and 411.4 Hz. The MAC values between each of the DIC rows and the CSLDV shapes are shown in Table 27.2 along with the frequency errors previously discussed. Separate MAC values were computed for the upper and lower row of computed 3D-DIC measurement points compared with CSLDV to show the consistency of 3D-DIC measurements across the entire surface of the beam. It is noted that MAC values for modes 1 and 2 are above 0.99 showing excellent correlation

Table 27.2 Modal comparison

	Mode	f_n AVG modal hammer test, Hz	% Change between pre- and postexperiment modal hammer tests	f_n CSLDV, Hz	% Error CSLDV	f_n DIC, Hz	% Error DIC	MAC upper	MAC lower
Sinusoidal	1	71.75	−0.70	71.24	−0.7112	71.30	−0.6269	0.9993	0.9997
	2	204.35	−0.49	204.33	−0.0117	204.50	0.0747	0.9968	0.9994
	3	411.45	−0.12	411.05	−0.0972	411.39	−0.0134	0.5381	0.7762
Random	1	72.15	−2.82	73.99	2.5554	73.00	1.1712	0.9988	0.9990
	2	204.85	−1.23	205.03	0.0864	205.35	0.2420	0.9984	0.9990
	3	412.05	−0.85	411.94	−0.0268	414.63	0.6260	0.9891	0.9883
	4	675.9	−0.52	675.58	−0.0471	676.38	0.0716	0.9376	0.9583

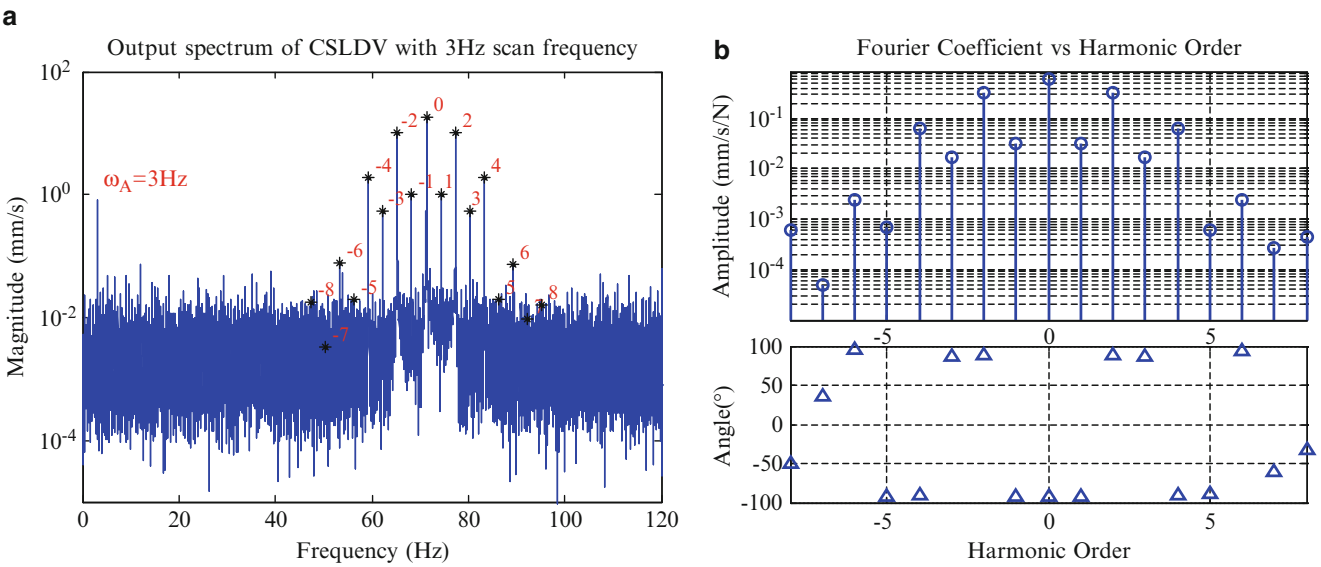

Fig. 27.5 Output spectrum for CSLDV

between CSLDV and high-speed 3D-DIC; however, due to the small displacements measured at 411.4 Hz, high-speed 3D-DIC begins to exhibit larger errors in the mode shape, which is shown in Fig. 27.6c, leading to MAC values 0.5381 and 0.7762. Additionally an asymmetry in the mode shape, where a larger amplitude of displacement is observed on the left end of the beam, is seen in mode 2 and 3, which is believed a result of asymmetry of the boundary conditions or an initial curvature in the beam that is below the measurable range of the 3D-DIC system. In either case, the asymmetry is undetectable until the dynamic response is observed with the large measurement resolution.

It is also important to note that while the smooth nature of the CSLDV mode shapes seems to suggest that they are infallible, they are in fact an approximation of the true mode shapes obtained by expanding them in a Fourier series of the time-varying scan pattern. As mentioned previously, 13 clearly dominant harmonics (i.e. $n = -6$ to 6) were observed for the first mode. The neglected harmonics were at least a few orders of magnitude smaller than the dominant ones, so one would be inclined to have high confidence in that shape. For example, if $n = -8$ to 8 were used to reconstruct the first bending mode shape, the maximum change in the shape is only 0.068 % with respect to the shape reconstructed using $n = -6$ to 6. Furthermore, because the laser is scanning along a line with CSLDV, when the measurements are noisy, the mode shapes measured on the forward and backward parts of the sweep tend to differ giving an indication of the error. Here, the forward and backward sweeps overlay completely suggesting that the shapes were quite accurate.

27.4.3 Natural Frequencies and Damping/Mode Shapes from Random Excitation

Band limited random noise over the range of 10–800 Hz was used to excite the first 4 modes of the clamped-clamped beam. For this experiment, a 9 Hz scan frequency was found to be preferable to help prevent the neighboring harmonics of each mode from blending together. The actual scan frequency ends up varying a little from what is commanded, for example, the scan frequency measured in the mirror displacement signals for this case was 9.0007 Hz. An accurate scan frequency is critical in this process since the phase error may accumulate especially when the time histories are long. The following plots show are the force spectrum and the output power spectrum (Fig. 27.7).

The random response data measured with the CSLDV and high-speed 3D-DIC was processed using AMI to identify the natural frequencies and mode shapes. For CSLDV, this included mode shapes from all identified sidebands, and the following figures show the fitted composite harmonic power spectrum around 73 Hz. For high-speed 3D-DIC, the response data was averaged 45 times with a block size of 5,000 samples and a 50 % overlap. The resulting response spectrums were then loaded into AMI to extract natural frequencies and mode shapes (Fig. 27.8).

The identified mode shapes obtained from the band limited random excitation are compared in Fig. 27.9. Figure 27.9a, b is the comparison of the identified modes at 72.15 Hz and 205.4 Hz between CSLDV and high-speed 3D-DIC, the mode shapes agree well, with computed MAC values above 0.99 for both modes. Figure 27.9c shows the third mode at 414.6 Hz, which has computed MAC values of 0.9891 and 0.9883. The measured random excitation was shown to excite the 3rd mode

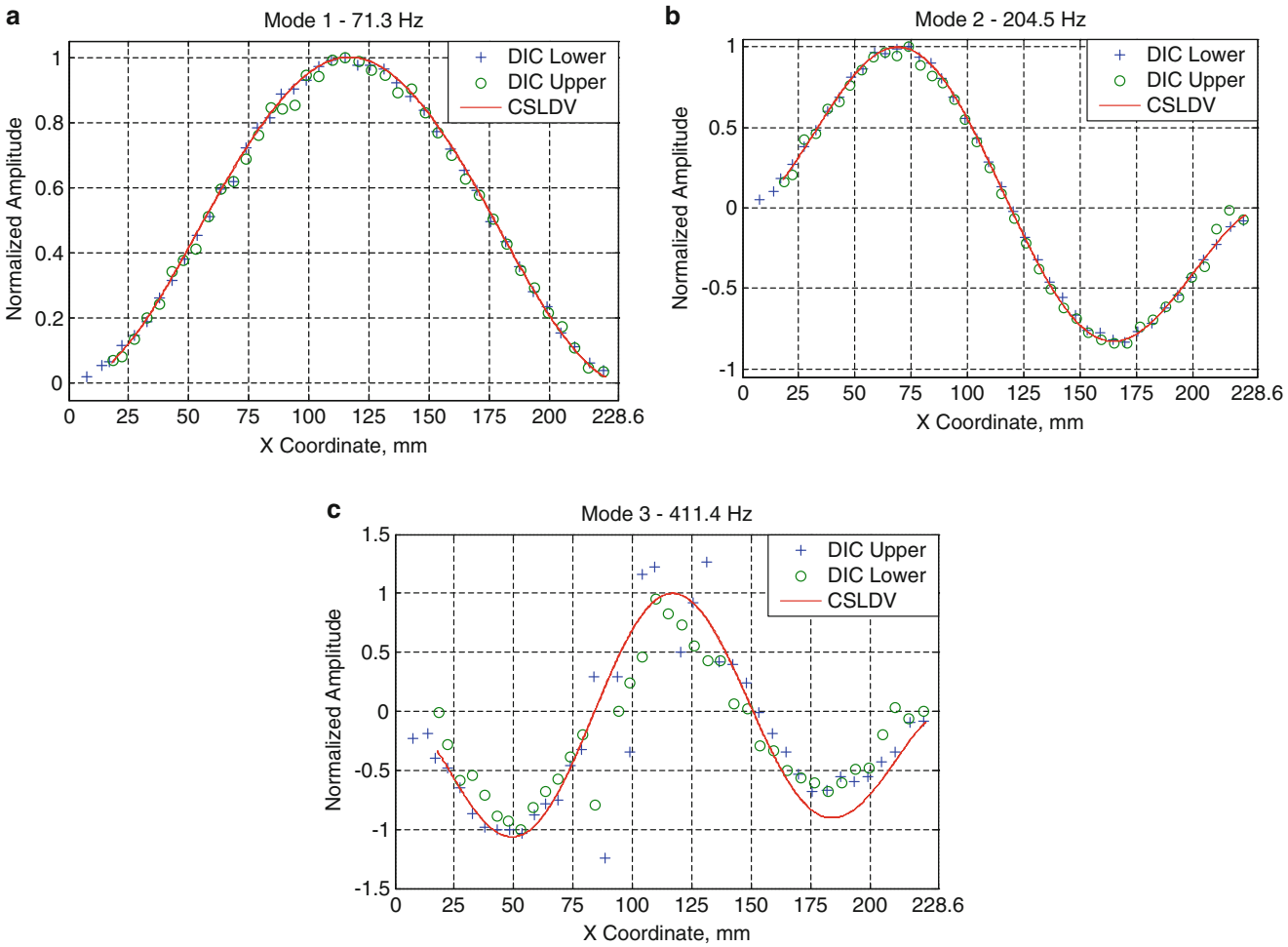

Fig. 27.6 Modes shapes from steady state excitation. (**a**) Mode 1 at 71.3 Hz, (**b**) Mode 2 at 204.5 Hz, and (**c**) Mode 3 at 411.4 Hz

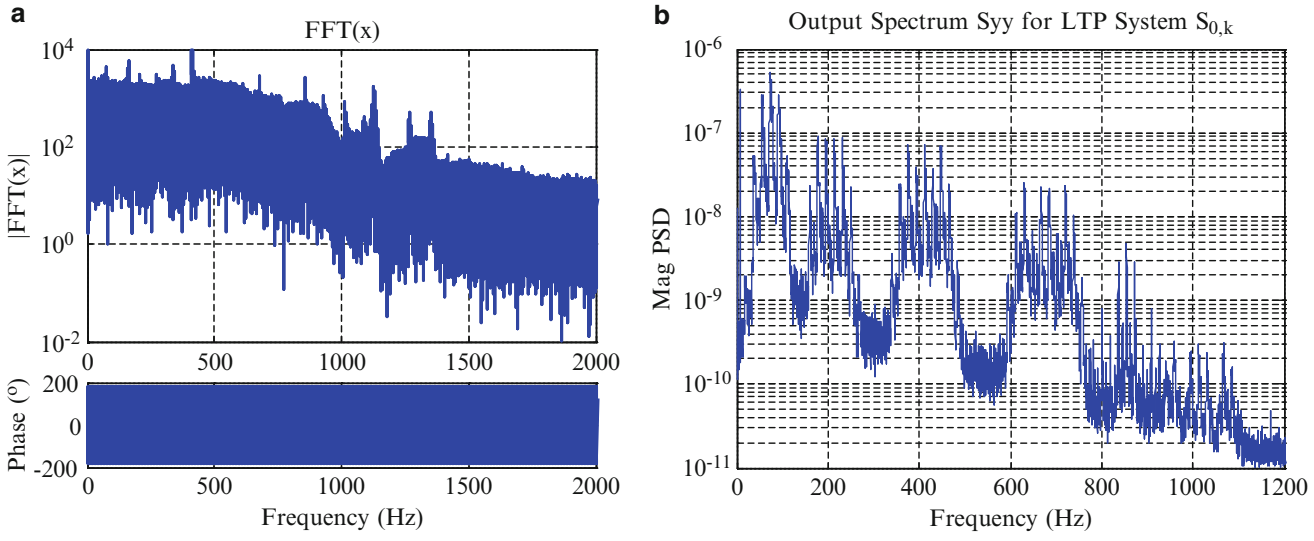

Fig. 27.7 Force spectrum and output power spectrum

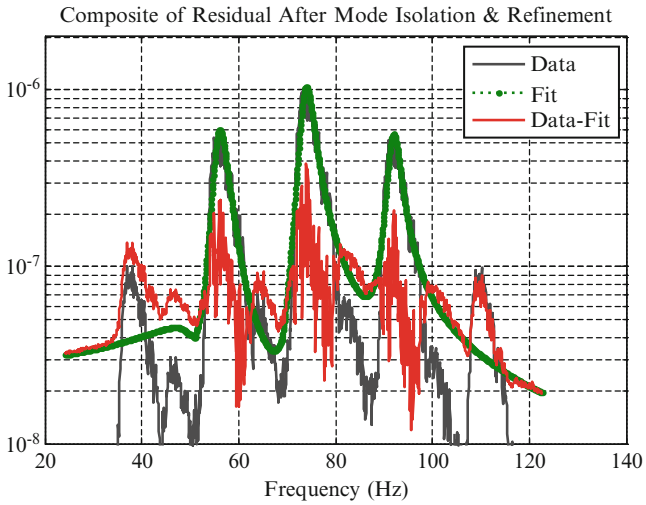

Fig. 27.8 Results of AMI mode isolation of the composite harmonic power spectrum from CSLDV measurement

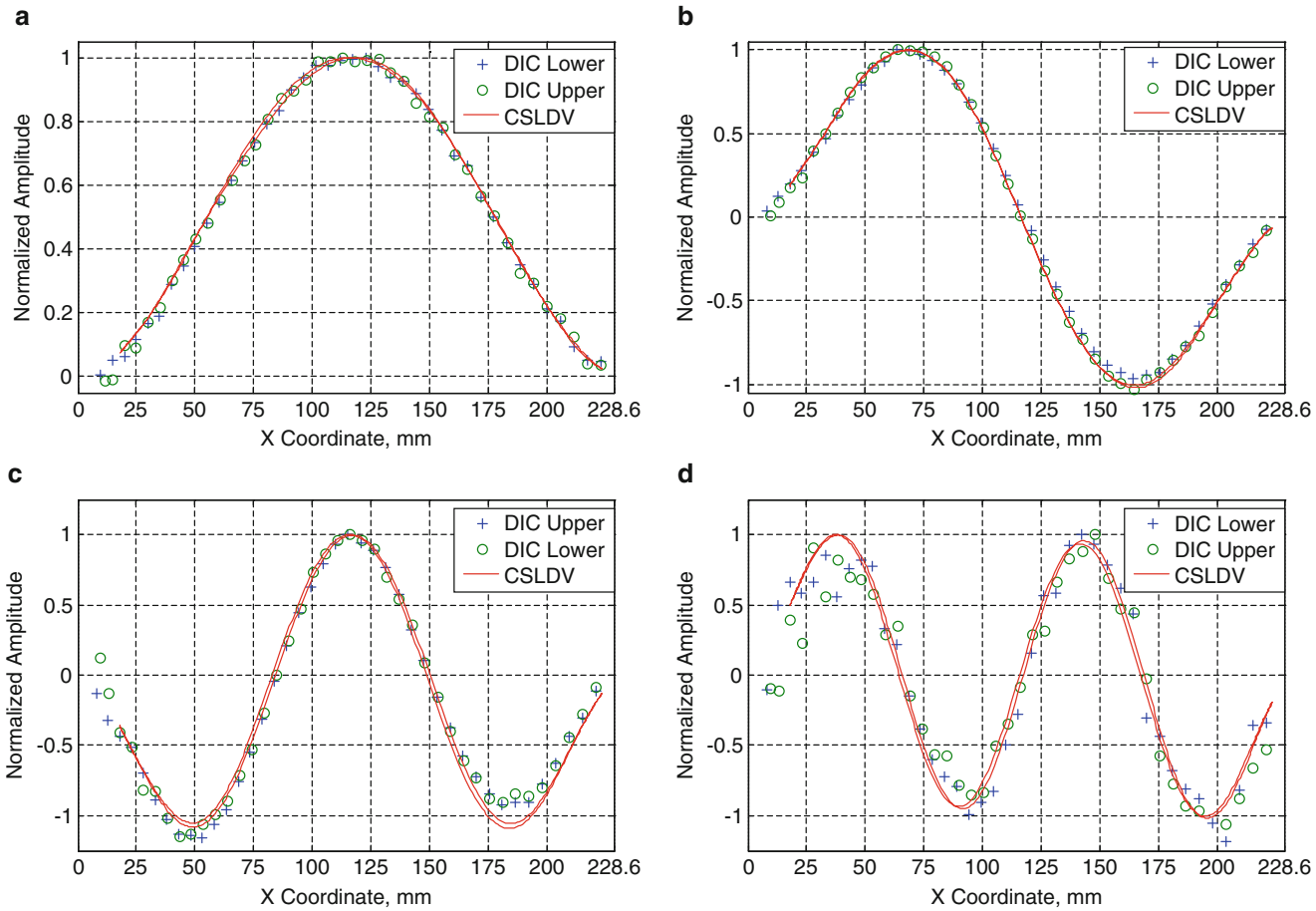

Fig. 27.9 Modes shapes from random excitation. (**a**) Mode 1 at 74.5 Hz, (**b**) Mode 2 at 205.4 Hz, (**c**) Mode 3 at 414.6 Hz, and (**d**) Mode 4 at 676.4 Hz

better than the use of a steady state sine wave as exhibited by the shape comparison and MAC value. Also, the asymmetry seen in the steady state sine dwell was seen with high-speed 3D-DIC; however, CSLDV did not capture the same asymmetry which could be a result of the shifting frequencies or expected shifting boundary conditions. Results of mode 4 are shown in Fig. 27.9d and computed MAC values of 0.9376 and 0.9583 were obtained for lower and upper 3D-DIC measurement locations, respectively. Again, as higher frequencies are measured, the smaller displacements lead to a greater observed noise with 3D-DIC as observed in the plot of mode 4.

27.5 Conclusion

Modes shapes and natural frequencies of a clamped-clamped flat steel beam were identified using CSLDV and high speed 3D-DIC. Natural frequencies were also identified using single-input single-output modal hammer testing for comparison with CSLDV and high speed 3D-DIC. A maximum frequency error of 2.56 % for CSLDV and 1.17 % for high speed 3D-DIC was observed when compared with the modal hammer tests. Throughout testing, single-input-single-output modal hammer tests showed that the natural frequencies shifted a maximum of 2.8 %. So, it is concluded that the frequency error between the modal hammer tests compared with CSLDV and 3D-DIC is largely due to the experimental setup instead of the measurement techniques. Additionally, inconsistencies with the clamped boundary conditions were identified with an asymmetry seen in the second and third mode shapes as measured with both CSLDV and 3D-DIC. Measurement error is dismissed as a cause since each measuring technique independently identified the asymmetry from the sinusoidal excitation test. For the random excitation experiment, the mode shape difference in the second and third mode is concluded to be from changing experimental conditions throughout the test since CSLDV and 3D-DIC are not measured simultaneously. Future work with an improved experimental setup is needed for further comparison, but it is shown that both techniques exhibit the ability to capture a high spatial resolution measurement of the clamped-clamped beam when subjected to steady state sinusoidal and band limited random excitations.

CSLDV was able to measure 1,708 points for the steady state sine excitation and 570 points for the random excitation. However, the information in the measurement is not governed by the number of points used to define the shape but by the number of Fourier coefficients that can be identified to describe the time-varying shape. In fact, decreasing the sample rate, and hence the number of points, has sometimes been found to increase the resolution of the measurement. An additional consideration with CSLDV is the measurement grid, which is dependent on the choice of a periodic scan signal and by the location of the laser on the surface, which is determined by a curve fit of the stepped galvo-motor signal. If a more complex 2-D grid of measurement locations is required, patterns following a Lissajous curve would be needed and testing time will increase. One benefit CSLDV has over high-speed 3D-DIC is the ability to measure at large stand off distances and maintain accuracy over larger test specimens; however, the maximum stand off distance is laser dependent and the measurement is limited to motion along the scan path and in the direction of the incident laser beam. Current LDVs clearly have much higher measurement resolution than DIC, down to tens of nanometer/second velocities or picometer displacements. Some of that resolution can be lost to speckle noise when scanning in a CSLDV mode, and yet in this study CSLDV was still clearly preferable for higher modes where the displacements were small.

High speed 3D-DIC was computed with two rows of 41 points for both excitations; however, a denser measurement grid can be obtained if needed since the images were stored. For the given field of view and beam geometry, 2,500 points can be computed in a 2D grid across the surface of the beam and the measurement resolution is independent of measurement duration or excitation type. (In CSLDV, the spatial information is captured in empty regions of the frequency band, and hence one must consider the input type, scan frequency, speckle noise, and the properties of the system to successfully capture measurements.) The spatial resolution of the acquired mode shape measured with high speed 3D-DIC is dependent on the stand off distance and the camera resolution; therefore, if more accurate measurements are needed, the camera setup needs to be moved closer to the test specimen, or a higher resolution camera is needed. Additionally, since high frequencies correspond to smaller displacements, high-speed 3D-DIC loses ability to measure mode shapes at higher frequencies. 3D-DIC mode shapes do appear nosier when compare with those measured with CSLDV; however, this is largely due to the fact that each measurement point is independent and subject to speckle pattern variations instead of dependent on a periodic signal. One benefit high-speed 3D-DIC has over CSLDV is the ability to provide a 2D grid of measurement points equally spaced across the specimen surface that measures the three dimensional deformations providing near full-field measurements in all deformation axes. Indeed, with 3D-DIC one can capture the in-plane motions of the surface even more accurately than the out-of-plane motions, whereas CSLDV can only capture the motion along the axis of the incident laser beam.

Both techniques can provide dense measurements along surfaces, as long as each technique can “see” the surface. To provide accurate measurements, both techniques require surface preparation, unless the material used for the test piece fulfills specific requirements (e.g. a random pattern for 3D-DIC and a sufficiently reflective pattern for CSLDV). For DIC, this surface preparation is especially important when response levels are small, or in a structure’s linear range. For CSLDV, surface preparation becomes more important when the vibration amplitude becomes small relative to speckle noise, and also as the laser standoff distance (or field of view) increases.

Finally, this study has illustrated that when full-field velocities or displacements are measured rather than simply motion at a few points, inconsistencies in the dynamic behavior (e.g. asymmetries in mode shapes) of the structure under test can be identified and provide insight to modeling and predicting dynamic behavior. Here, the CSLDV and DIC shapes revealed asymmetry in the 2nd and 3rd bending mode shapes which was probably due to (unmodeled) asymmetry in the boundary conditions. If a traditional test were performed with only a few measurement points, one would not be likely to detect this, nor would they have sufficient information to update the model to account for it.

References

1. Schwingshackl CW, Stanbridge AB, Zang C, Ewins DJ (2007) Full-field vibration measurement of cylindrical structures using a continuous scanning LDV technique. Presented at the 25th international modal analysis conference (IMAC XXV), Orlando, Florida, 2007
2. Stanbridge AB, Ewins DJ (1999) Modal testing using a scanning laser Doppler vibrometer. Mech Syst Signal Process 13:255–270
3. Stanbridge AB, Martarelli M, Ewins DJ (2004) Measuring area vibration mode shapes with a continuous-scan LDV. Measurement 35:181–189
4. Martarelli M (2001) Exploiting the laser scanning facility for vibration measurements. Ph.D., Imperial College of Science, Technology & Medicine, Imperial College, London
5. Stanbridge AB, Khan AZ, Ewins DJ (2000) Modal testing using impact excitation and a scanning LDV. Shock Vib 7:91–100
6. Allen MS (2009) Frequency-domain identification of linear time-periodic systems using LTI techniques. J Comput Nonlinear Dynam. 4(4). DOI 10.1115/1.3187151
7. Yang S, Sracic MW, Allen MS (2012) Two algorithms for mass normalizing mode shapes from impact excited continuous-scan laser Doppler vibrometry. J Vib Acoust 134:021004
8. Wereley NM (1991) Analysis and control of linear periodically time varying systems. Ph.D., Department of Aeronautics and Astronautics, Massachusetts Institute of Technology, Cambridge
9. Wereley NM, Hall SR (1991) Linear time periodic systems: transfer functions, poles, transmission zeroes and directional properties. In: Presented at the proceedings of the 1991 American control conference, Boston, MA, USA, 1991
10. Wereley NM, Hall SR (1990) Frequency response of linear time periodic systems. Proceedings of the 29th IEEE Conference, Honolulu, HI, USA, pp 3650–3655 DOI:DOI 10.1109/CDC.1990.203516
11. Yang S (2013) Modal identification of linear time periodic systems with applications to continuous-scan laser Doppler vibrometry. Ph.D., Engineering Physics, University of Wisconsin-Madison
12. Schmidt TE, Tyson J, Galanulis K, Revilock DM, Melis ME (2005) Full-field dynamic deformation and strain measurements using high-speed digital cameras, Proceedings of the SPIE, pp 174–185, DOI 10.1117/12.567142
13. Tiwari V, Sutton MA, Shultis G, McNeill SR, Xu S, Deng X, Fourney WL, Bretall D (2009) Measuring full-field transient plate deformation using high speed imaging systems and 3D-DIC. In: Proceedings of the society for experimental mechanics annual conference, Albuquerque, 2009
14. Niezrecki C, Avitabile P, Warren C, Pingle P, Helfrick M (2010) A review of digital image correlation applied to structural dynamics. Am Inst Phys Conf Proc 1253:219–232
15. Helfrick M (2011) 3D digital image correlation methods for full-field vibration measurement. Mech Syst Signal Process 25:917–927
16. Warren C, Niezrecki C, Avitabile P, Pingle P (2011) Comparison of FRF measurements and mode shapes determined using optically image based, laser, and accelerometer measurements. Mech Syst Signal Process 25:2191–2202
17. GmbH (2011) Aramis, 6.3.0 edn. Braunschweig, Germany
18. GmbH (2011) IVIEW real time sensor, 6.3.0 edn. Braunschweig, Germany
19. Yang S (2013) Modal identification of linear time periodic systems with applications to continuous-scan laser Doppler vibrometry. Ph.D., Engineering Physics, University of Wisconsin-Madison
20. Yang S, Allen MS (2012) Output-only modal analysis using continuous-scan laser Doppler vibrometry and application to a 20 kW wind turbine. Mech Syst Signal Process 31:2011
21. Sutton MA, Orteu JJ, Schreier H (2009) Image correlation for shape, motion, and deformation measurements: basic concepts, theory, and applications. Springer New York, DOI 10.1007/978-0-387-78747-3
22. Gordon RW, Hollkamp JJ, Spottswood SM (2003) Non-linear response of a clamped-clamped beam to random base excitation. Presented at the VIII international conference on recent advances in structural dynamics, Southampton, United Kingdom, 2003
23. Gasparoni A, Allen MS, Yang S, Sracic MW, Castellini P, Tomasini EP (2010) Experimental modal analysis on a rotating fan using tracking-CSLDV. Presented at the 9th international conference on vibration measurements by laser and noncontact techniques, Ancona, Italy, 2010
24. Yang S, Allen MS (2012) A lifting algorithm for output-only continuous scan laser Doppler vibrometry. Presented at the 53rd AIAA structures, structural dynamics, and materials conference, Honolulu, Hawaii, 2012
25. Martin P (2010) Uncertainty due to speckle noise in laser vibrometry. Doctor Thesis, Wolfson School of Mechanical and Manufacturing Engineering, Loughborough University